LUND UNIVERSITY

The impact of mass transfer and interfacial expansion rate on droplet size in membrane emulsification processes

Rayner, Marilyn; Trägårdh, Gun; Trägårdh, Christian

[Link to publication]

The impact of mass transfer and interfacial expansion rate on droplet size in membrane emulsification processes

Marilyn Rayner*, Gun Trägårdh, Christian Trägårdh

Department of Food Technology, Engineering and Nutrition, Lund University, P.O. Box 124, 221 00 Lund, Sweden

Abstract

In membrane emulsification, especially under conditions where droplets are forming with a narrow droplet size distribution, it is conjectured that the interfacial phenomena are determining the emulsification result. The process parameters of continuous phase flow and dispersed phase flux were analysed from the perspective of how they could be affecting the interfacial tension of the growing droplet. This work first reviews the applicability of current droplet formation models (force balance and spontaneous transformation based (STB)), describes the interfacial transport of surfactant molecules to an expanding oil–water interface, and models the flow of dispersed phase through a pore using MATLAB. The data from these calculations are then applied in a model to predict the final size of the droplets, which includes dynamic effects of mass transfer and expansion rate.

The droplet detachment mechanism in membrane emulsification was modelled from the point of view of Gibbs free energy. An interactive finite element program called the surface evolver was used to test the model. A program was written and run in the surface evolver, which allows the user to track the droplet shape as it grows, to identify the point of instability due to free energy, and thus predict the maximum stable volume (MSV) attached to the pore. The final droplet size was found by applying a pressure pinch constraint (PPC), which is based on the division of the surface into two volumes, a droplet and a segment, which remains attached to the pore mouth. The relative size of these two volumes is such that the resulting radii of curvature of the droplet will maintain an equal Laplace pressure across the surface of both volumes. Predicted droplet sizes were compared to experimental data from the literature. It was found that changes in surfactant coverage caused by mass transfer coupled to the expansion rate of the oil–water interface have a significant and predictable effect on the final droplet size in membrane emulsification.

The extent of the influence of the dispersed phase flux on dynamic interfacial tension was quantified using a dimensionless parameter, the mass transfer expansion ratio (MER). The MER can be used to predict the effect of increasing the depletion of surfactant on the relative final droplet size in membrane emulsification. This new insight into the role mass transfer and surface expansion play in membrane emulsification allows us to now predict à priori the final droplet size that would form for a particular set of conditions, and can lead to better process design methods in the future.
© 2005 Elsevier B.V. All rights reserved.

Keywords: Membrane emulsification; Mass transfer; Surface evolver; Modelling; Droplets

1. Introduction

There has been an increasing interest in a new technique for making emulsions known as membrane emulsification in which the continuous phase is pumped along the membrane and sweeps away dispersed phase droplets forming from pore openings as shown in Fig. 1. The key feature of the membrane emulsification process, which sets it apart from conventional emulsification technologies, is that the size distribution of the resulting droplets is primarily governed by the choice of membrane and not by the development of turbulent droplet break up [1]. The main advantages of membrane emulsification are the possibility to produce droplets of a defined size with a narrow size distribution, low shear stress, the potential for lower energy consumption, and simplicity of design [2].

* Corresponding author. Tel.: +46 46 222 9820; fax: +46 46 222 46 22.
E-mail address: marilyn.rayner@livstek.lth.se (M. Rayner).

Nomenclature

a	droplet size to pore size ratio
A	surface are of droplet (m^2)
C	surfactant concentration (mol/m^3)
C_{bulk}	bulk surfactant concentration (mol/m^3)
C_s	sub-surface surfactant concentration (mol/m^3)
D	diffusion coefficient ($mol/m^2\,s$)
D_{drop}	droplet diameter (m)
D_{pore}	pore diameter via mercury porosimetry measurements (m)
$E_{Laplace}$	energy associated to Laplace pressure (J)
E_{pore}	energy of the pore (J)
E_{surf}	surface energy (J)
E_{Total}	total energy from surface evolver (J)
$G, \Delta G$	Gibbs free energy, change in free energy (J)
H	mean curvature (1/m)
k	Boltzmann's constant 1.380×10^{-23} (J/K)
k_{cts}	continuous phase mass transfer coefficient (m/s)
k_x	corrects for a sphere in contact with a solid wall equals 1.7
L_{eff}	effective length of membrane pores including tortuosity (m)
MER	mass transfer expansion ratio
MSV	maximum stable volume (m^3)
P	pressure (Pa)
$P_{applied}$	applied pressure on dipersed phase (Pa)
$P_{attached}$	pressure across attached surface (Pa)
P_{break}	pressure inside a detached droplet (Pa)
P_{cap}	capillary pressure (Pa)
$P_{critical}$	critical pressure inside a pore or across a membrane (Pa)
P_{cts}	pressure in continuous phase (Pa)
P_{drop}, P_{drop_new}	pressure inside a detached droplet (Pa)
P_{eff}	effective trans-membrane pressure (Pa)
P_{hyd}	pressure drop across membrane due to flow resistance (Pa)
$P_{Laplace}$	Laplace pressure of drop or interface (Pa)
P_{tm}	trans-membrane pressure (Pa)
Q	flow rate of dispersed phase through pore (m^3/s)
R	universal gas constant 8.314 (J/mol K)
R	radius of a sphere in Eq. (30) (m)
R_{break}	radius of detaching droplet (m)
R_c, R_{c1}, R_{c2}	radii of curvature or dimension of major and minor axis (m)
R_{drop}	radius of drop that breaks off [m]
R_g	radius of gyration of a polymer in solution (nm)
R_{max}, R_{min}	local maximum and minimum radii of curvature (m)
Re	Reynolds number
S	surface area (m^2)

Sc	Schmidt number
t	time (s)
T	temperature (K)
U	velocity (m/s)
V	volume (m^3)
$V_{attached}$	volume of attached surface (m^3)
$V_{droplet}$	volume of detaching droplet (m^3)
V_{MSV}	maximum stable volume (m^3)
W	work (J)
z	distance from oil–water interface (m)

Greek symbols

α	constant equal to $2\,Re^{-1/8}$
δ	boundary layer thickness (m)
$\dot{\varepsilon}$	expansion rate (m^2/s)
γ	interfacial tension (N/m)
$\gamma_{detachement}$	interfacial tension of droplet at detachment (N/m)
$\gamma_{equilibrium}$	interfacial tension at equilibrium (N/m)
γ_o	interfacial tension of clean oil–water interface (N/m)
Γ	interfacial coverage of surfactant (mol/m^2)
Γ_{max}	maximum interfacial coverage of surfactant (mol/m^2)
Γ^*	non-dimensional interfacial coverage of surfactant
$\dot{\Gamma}_{expansion}$	interfacial flux due to expansion ($mol/m^2\,s$)
$\dot{\Gamma}_{transfer}$	interfacial flux due to mass transfer ($mol/m^2\,s$)
ρ	density (kg/m^3)
T	contact energy density (J/m)
μ	viscosity (Pa s)
θ, θ_c	contact angle (°)
Θ	dilation rate (1/s)
τ_{wall}	wall shear stress [Pa]
Ω	flow resistance [Pa s/m^3]

The interfacial tension, membrane properties (i.e. mean pore size, membrane thickness and porosity), dispersed phase viscosity, and applied dispersed phase pressure determine the flow rate through the micro-porous membrane. As a droplet is pressed into the continuous phase, a new interface is created and surfactant molecules act at this surface to reduce the tension over time. Membrane emulsification differs from conventional emulsification processes in that the droplet formation time is of the same order of magnitude as the reduction in surface pressure via dynamic interfacial tension of common food emulsifiers [3]. The effect of emulsifiers is further complicated by the fact that droplet expansion and adsorption at the interface are coupled, thus both the rate at which expansion and detachment mechanisms act, as well as how fast emulsifiers adsorb to the growing interfacial area become relevant over the time scales involved. We will refer to these emulsifiers as surfactants (surface active agents), as it is their action of reducing interfacial tension, rather than conferring

Dispersed phase is pressed through the membrane

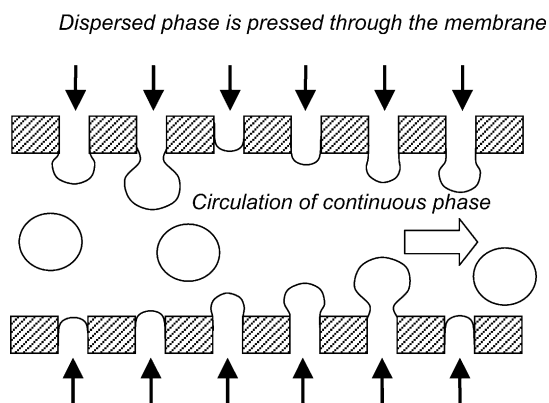*Circulation of continuous phase*

Fig. 1. Principle of membrane emulsification.

long-term emulsion stability, that is the main focus of this work.

In the literature there has been a considerable amount of descriptive work performed on the membrane emulsification process. For extensive and recent reviews on membrane emulsification consult Joscelyne and Trägårdh [4], Charcosset et al. [5] and Gijsbertsen-Abrahamse et al. [7]. Other authors have described droplet formation depending by considering the type of mechanisms causing the droplets to detach and or the systems sensitivity to operating conditions [8–10]. There are two main detachment mechanisms described in the literature: spontaneous transformation-based (STB) droplet formation and, shear induced droplet formation. Spontaneous transformation-based droplet formation describes situations where the droplets are formed without the necessity of a cross flow and droplet break off occurs due to the minimization of free energy [11,12]. Shear induced droplet formation describes conditions where the flow of the continuous phase affects the size and distribution of the droplets [6,8,13,14] and is generally modelled using a force balance approach.

A wide variety of results have been reported in the literature with respect to emulsion characteristics in membrane emulsification systems. The droplet size to pore size ratio, has been found to range from approximately 3 to 15 [4,5] for oil-in-water emulsions and the size distributions have been in some cases mono-dispersed, but with others showing over 50% coefficient of variation [6]. Size and size distribution are the parameters of an emulsification system, which determines the products quality as fitness for its intended use, and thus are essential to control and predict. To achieve this one needs to know what specific process conditions yield particular emulsification outcomes.

2. Structure and objectives of the paper

During membrane emulsification it is inferred that the interfacial phenomena are having a large impact on the emul-

sification result. With this in mind the above-mentioned process parameters of continuous phase flow and dispersed phase flux were analysed from the perspective of how they could be affecting the interfacial tension of the growing droplet. Therefore, the objects of this work are to: review the applicability of current droplet formation models (force balance and spontaneous transformation based), describe the interfacial transport of surfactant molecules to an expanding oil–water interface, model the flow of dispersed phase through a pore, to calculate the subsequent expansion rates and dynamic interfacial tension as the droplet grows into the continuous phase. The data from these calculations are applied in a model to predict the final size of the droplets, which includes the effects of mass transfer and expansion rate. The final section consists of simulation results using the model, which are compared to literature data, discussed, and some general conclusions are drawn. It is hoped that this type of analysis and modelling which underlies the importance of mass transfer in membrane emulsification, and in the future can lead to better process design methods beyond a trial and error approach.

3. Shear induced droplet formation according to the force balance model

The size of droplets when they detach from the membrane or micro-channel depends on the above mentioned process parameters, which have been evaluated by associating them to forces which act on the system [1,5,15–18]. The relative magnitude of these forces change as the droplet increases in size and has been plotted in the literature [1,12,15]. It has been shown that for micron scale droplets the inertia and buoyancy forces are approximately 9 and 6 orders of magnitude smaller, respectively than the drag and interfacial tension forces and therefore, can be neglected in the force balance model. The interfacial tension force ($F\gamma$), represents the effects of dispersed phase adhesion around the edge of the pore opening and is the key retaining force during droplet formation, where as viscous drag force (F_D), is created by the continuous phase flowing past the droplet parallel to the membrane surface. The characteristic parameter used to discuss the effect of the flowing continuous phase is the wall shear stress. Previous studies have shown that the droplet size decreases as the wall shear stress increases [5,7,19]. One popular explanation of this phenomenon is that the flowing continuous phase creates the drag force that pulls the droplets away from the pore mouths after reaching a certain size [15]. According to this approach, the point at which the droplet detaches occurs when the sum of these forces acting on it equals zero, yielding the following equation by solving for the drop diameter:

$$D_{\text{drop}} = \sqrt{\frac{4\gamma D_{\text{pore}}}{6k_x \tau_{\text{wall}}}} \tag{1}$$

where D_{pore} is the pore diameter, γ is the interfacial tension, and $k_x = 1.7$ corrects for a sphere in contact with a solid wall
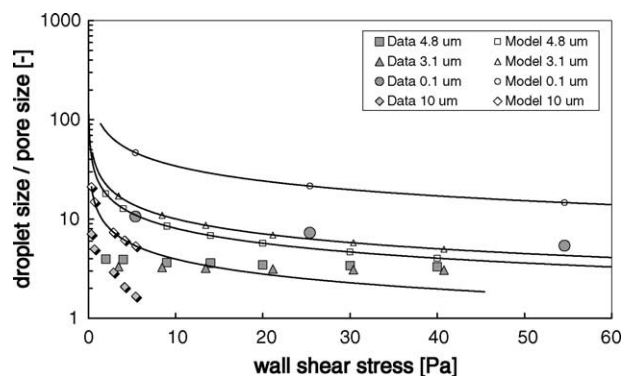
Fig. 2. Droplet size to pore size ratio versus wall shear stress. Lines are the size predicted by the force balance model (open symbols). Data (shaded symbols) 4.8 and 3.1 μm pore diameter, 2 wt.% Tween 80 [23] 0.1 μm pore diameter, 1% wt SDS (Berot et al. Trans IChemE 81 Part A (2003) 1077) 10 μm pore diameter, 0.3% SDS [19].

[1]. There have been cases in reported the literature where the force balance model has successfully described experimental findings. For example, Peng and Williams formed droplets ranging from 137 to 430 μm, depending on the cross flow rate, using a capillary that was 45 μm in diameter. Van Rijn [20] also report good agreement with the force balance mode using 4 μm diameter pores forming droplets 28–120 μm in diameter but have very large droplet size to pore size ratios averaging 16 with a maximum of 30 at the lowest wall shear rates. However, with the exception of the aforementioned cases, the droplet sizes predicted by this equation are generally not in accordance with experimental results reported in the literature. Droplet size predictions using the force balance model for pores smaller than 10 μm are shown in Fig. 2. The notable feature of this plot is how much the model over predicts drop size at low to moderate wall shear stresses, for example, the average error on predictions with wall shear stresses less than 20 Pa is 214%. On the other hand, if we consider the case with the lowest error (22%), a 4.8 μm SPG membrane, 40 Pa wall shear stress and 8 mN/m interfacial tension [21] one can calculate that the Laplace pressure of these droplets is on the order of 6700 Pa, i.e. more than 160 times larger than the shear stress which is supposed to be detaching them. The point is that the droplet has a much higher pressure than the pressure exerted by the drag forces of the continuous phase, so then how would the continuous phase be able to significantly deform the droplet leading to a shear induced detachment? Despite the effect of the continuous phase flow on reducing the size of the droplets, the question still arises: how are these droplets detaching at all?

4. Spontaneous transformation-based droplet formation

The answer to droplet detachment question may lie in the interfacial energy. The effects of interfacial tension have been previously regarded as a retaining mechanism, but may in fact provide the actual means to drive droplet detachment. Sugiura et al. [22] presented a mechanism for interfacial tension driven droplet formation. This mechanism termed "Spontaneous Transformation Based" droplet formation is described by considering the Gibbs free energy of the system. In their set-up the droplet was deformed by the rectangular geometry of the micro-channel causing it to have a disc-like shape, which is unstable from the view point of Gibbs free energy, since it has a much greater interfacial area than a sphere of equivalent volume. The ability for a droplet to spontaneously form was calculated from the reduction in total interfacial area from before and after the droplet forms through estimating the interfacial areas from video images obtained using the set-up described in Kawakatsu et al. [21]. They found that the geometry of the micro-channel played a critical role in STB droplet formation since it is essential that the droplet is deformed from its spherical, lowest energy shape. This type of droplet deformation does not solely take place in micro-channel emulsification, but is also observed in Shirasu porous glass (SPG) membrane emulsification and in arrays of straight through holes in silicon plates. Sugiura et al.'s estimation of the free energy of droplet formation showed that STB droplet formation was favourable, and could predict droplet diameter using geometric and regression analysis to obtain two fitting parameters from the experimental data. Their prediction curve correlated well with their measured data having a mean relative error of 4.6% [22].

Rayner et al. [12] used this free energy approach to model droplet formation from micro-fabricated membranes under quiescent conditions. The input to this model was contact angle, interfacial tension, and pore geometry. Furthermore, in contrast to previous work, this model did not use regression analysis or any empirical fitting parameters to predict droplet size. This modeling work was validated against experimental data with an average estimation error of 8%. The present work extends this model to include the dynamic effects of mass transfer and dispersed phase flux on the final droplet size.

5. Effects of wall shear stress and dispersed phase flux from the perspective of interfacial phenomena

As indicated above, it cannot be the drag force alone which acts to reduce the size of droplets forming under cross flow conditions. Another possible analysis is that as the wall shear stress increases, the thickness of the viscous boundary layer decreases and thus the rate of mass transfer of surfactant increases (calculation details for mass transfer rate are provided in Section 8). This in turn speeds up the reduction of the interfacial tension of the oil–water interface, and could in turn yield smaller relative droplet sizes. Fig. 3 shows the relationship between wall shear stress, reduction in the relative droplet size, and increases in the mass transfer rate. Although the hydrodynamic drag is not thought necessary in all cases for a droplet to detach, circulation of the continuous phase is
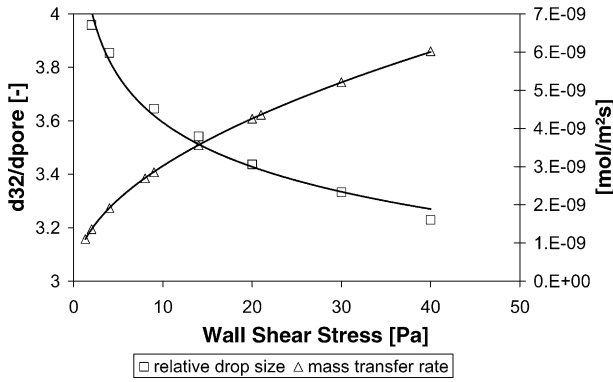
Fig. 3. Effect of wall shear stress on mass transfer rate and mean droplet size to pore size ratio (d32/dpore). Tween 80, 2%, 4.8 μm pore, data from [23].

still employed to carry away the formed droplets to prevent re-coalescence, as well as replenish the supply of surfactant to the membrane region.

In addition to continuous phase flow, the rate at which the dispersed phase is pressed through the membrane appears to play a crucial role. Several studies have found that there is an upper limit of dispersed phase flux at which the droplet size begins to increase under the same cross-flow conditions [9,10,23]. If the dispersed phase flux is further increased, the average droplet size begins to escalate and the coefficient of variation can increase by 10–20-fold [9,11]. From the above-mentioned analysis it can be justified that changes in the interfacial tension are the most likely and dominating phenomena causing the cross-over between different modes of droplet formation. The interfacial tension is increased by the creation of fresh interface as the droplet expands and lowers the coverage per unit area, and conversely the interfacial tension is lowered by new surfactant adsorbing from the continuous phase to the surface. Due to the interfacial phenomena's significant effect on droplet formation, it is important to know how the process conditions of continuous phase flow and dispersed phase flux are coupled though interfacial tension. The coupling of effects of these parameters has been considered empirically by De Luca et al. [24], however, further understanding and modelling is required.

6. Mass transfer and adsorption equations

The interfacial tension is calculated from the interfacial coverage, via isotherms. The theoretical equilibrium interfacial coverage can be calculated by Gibb's isotherm equation, where C_s is the subsurface concentration of surfactant in the continuous phase solution:

$$\Gamma = -\frac{1}{RT}\left(\frac{d\gamma}{d\ln C_s}\right) \tag{2}$$

The subsurface is not fixed but rather defined as a position in the bulk phase from, at an infinitely short distance from the interface where surfactant molecules can adsorb without further bulk transport. The Gibbs isotherm has a corresponding surface equation of state (Eq. (3)), which is based on thermodynamic adsorption assuming that activities may be given as concentrations and there is no interaction between adsorbed monomers [25].

$$\gamma = \gamma_0 - nRT\,\Gamma \tag{3}$$

where $n = 1$ for neutral molecules and $n = 2$ for ionics [26] and RT is the universal gas constant times the temperature in Kelvin.

The driving force of the transport is generated by the concentration gradient created as the bulk solution is depleted of surfactant molecules near the subsurface as they are transferred from the soluted to the adsorbed state [27]. The mass transfer equations used to describe the dynamic surface tension, via the interfacial coverage, follow the analysis presented by Joos [28].

$$\frac{d\Gamma}{dt} + \Theta\Gamma = D\left(\frac{\partial C}{\partial z}\right)_0 \tag{4}$$

where Γ is the surface coverage, Θ is the dilation rate, C is surfactant concentration and D is the diffusion coefficient. The $\Theta\Gamma$ term can be considered the flux due to expansion of the droplet and the $\partial C/\partial z$ the diffusion flux term due to mass transfer in the continuous phase, with a mass transfer coefficient k_{cts} and concentration difference ($C_{bulk} - C_s$).

$$\dot{\Gamma}_{expansion} = \Theta\Gamma_{(t)} \tag{5}$$

$$\dot{\Gamma}_{transfer} = D\left(\frac{\partial C}{\partial z}\right)_0 = k_{cts}(C_{bulk} - C_s) \tag{6}$$

$$\frac{d\Gamma}{dt} = \dot{\Gamma}_{transfer} - \dot{\Gamma}_{expansion} \tag{7}$$

Eq. (4) has been simplified from the general diffusion equation through the following assumptions and boundary conditions. Firstly, there is a local equilibrium between the interface adsorption and the subsurface concentration. Because of local equilibrium, the chemical potential must be equal at the subsurface and at the interface. The relation between these is given by the Gibbs adsorption isotherm. Secondly, the surface diffusion (parallel to the interface) is small and can be neglected as is the effect of the droplet's curvature on the diffusion, and finally that a gradient in adsorption corresponds to a gradient in interfacial tension that levels out very quickly due to the Maragoni effect [28].

Although we assume that there is a rapid local equilibrium between the subsurface and the interface we do not assume that the interface is a sink, but rather that it has some finite capacity for adsorption. If the interface were assumed to be a sink then the subsurface concentration should always be zero. Ward and Tordai were the first to take the capacity of the interface into account in their famous convolution integral [28]. In this work, the diffusion and coverage equations are solved numerically and the interfacial coverage is charted
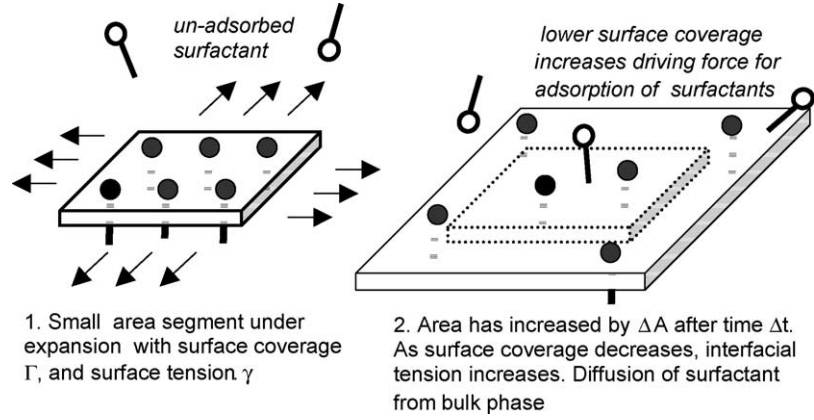
Fig. 4. Surface expansion and tension relaxation due to transport of surfactants.

over time. Therefore, to model this saturation effect we use Γ^* to scale the concentration gradient in the continuous phase.

$$\Gamma^* = \left(1 - \frac{\Gamma_{(t)}}{\Gamma_{max}}\right) \tag{8}$$

when $\Gamma_{(t)} = \Gamma_{max}$ the surface is "full" and the concentration gradient is zero, i.e. the concentration at the subsurface is equal to the bulk concentration, C_{bulk}, in the continuous phase. Similarly, when the interface is "empty" $\Gamma_{(t)} = 0$ the concentration gradient is at its maximum $C_s = 0$. This scaling idea is based on the Langmuir [29] isotherm, the most commonly used non-linear isotherm, which is founded on a lattice type model [25]. This adsorption isotherm's equation of state can be expressed by the Langmuir–Szyskowski relation [30].

$$\gamma = \gamma_o + RT\,\Gamma_{max} \ln\left[1 - \frac{\Gamma}{\Gamma_{max}}\right] \tag{9}$$

This equation of state gives smaller and smaller reductions in interfacial tension as the interface approaches full coverage. Likewise one would get ever decreasing slopes of chemical potential and concentration gradients as the surface becomes more saturated. Similarly in Eq. (6), rather than using $(C_{bulk} - C_s)$ for the concentration gradient and having to solve for C_s, we instead look at the degree of saturation which affects the chemical potential gradient driving further adsorption, and scale the maximum concentration gradient accordingly:

$$\dot{\Gamma}_{transfer} = k_{cts}(C_{bulk}\,\Gamma^*) \tag{10}$$

7. Surfactant coverage of an expanding surface

When a new droplet begins to grow from a pore, there is some surfactant already at the interface. However, because the area is increasing the surfactant surface coverage decreases, this in turn creates room for additional surfactant molecules to adsorb and leads to the transport of the surfactant to the subsurface. Determining the flux of surfactant is not enough in the case of an expanding droplet because the expansion

rate is dependent on the interfacial tension set by the surface coverage of surfactants. This is a coupled process governed by the transport of the surfactant from the bulk continuous phase to the subsurface where adsorption can occur, as well as the depletion due to the isotropic expansion of the interface.

We can derive $\dot{\Gamma}_{expansion}$ with the help of Fig. 4. The small segment of area has a surface coverage Γ_i and area S_i at time t_i. At time t_{i+1} after a small time increment $\Delta t = t_{i+1} - t_i$ the new area is $S_{i+1} = S_i + \Delta S$ and the new interfacial coverage is Γ_{i+1}. Since the change in surface coverage is caused by stretching alone:

$$\Gamma_{i+1} = \frac{\Gamma_i S_i}{S_{i+1}} = \frac{\Gamma_i S_i}{S_i + \Delta S}, \tag{11}$$

$$\dot{\varepsilon} = \frac{dS}{dt} = \frac{\Delta S}{\Delta t}, \tag{12}$$

$$\Gamma_{i+1} = \frac{\Gamma_i S_i}{S_i + \dot{\varepsilon}\,\Delta t}, \quad \text{and} \tag{13}$$

$$\dot{\Gamma}_{expansion} = \frac{\Delta\Gamma}{\Delta t} = \frac{\Gamma_{i+1} - \Gamma_i}{\Delta t}$$
$$= \left(\frac{S}{(S + \dot{\varepsilon}\,\Delta t)\,\Delta t} - \frac{1}{\Delta t}\right)\Gamma_{(t)}, \quad \text{thus} \tag{14}$$

$$\Theta = \left(\frac{S}{(S + \dot{\varepsilon}\,\Delta t)\,\Delta t} - \frac{1}{\Delta t}\right) \tag{15}$$

where S is the interfacial area and, $\dot{\varepsilon}$ is the surface expansion rate at time t. The rate of surface expansion is important in defining this problem as it represents depletion in terms of surface coverage of the surfactant in the transfer process.

8. Mass transfer coefficients

The mass transfer in the continuous phase, k_{cts}, is analysed by considering two cases; first at low wall shear rates where the process is dominated by molecular diffusion through an

"infinite" boundary layer, and then at moderate wall shear rates where both diffusion and flow convection are taken into account.

For a particular diffusion coefficient, droplet formation time, and boundary layer height, δ we can have a situation described using the Reynolds analogy if:

$$\frac{\delta^2}{Dt} < \pi \tag{16}$$

or alternatively penetration theory if:

$$\pi \leq \frac{\delta^2}{Dt} < \infty \tag{17}$$

Depending on which condition is fulfilled appropriate model is applied to determine k_{cts}.

8.1. How to describe the mass transfer at low wall shear rates: penetration theory

When the wall shear stress is low, this system can be modelled by penetration theory, which was proposed by Higbie [31]. If the depth of penetration is less than the total depth of the liquid boundary layer there is no significant error introduced by assuming that the total depth is infinite. The existence of velocity gradients within the fluids are ignored since surfactant transport takes place primarily by molecular diffusion when inside the viscous boundary layer. This penetration depth distance increases as a function of time as the continuous phase is depleted of surfactants as they are adsorbed to the surface. Since, the surfactant is assumed not to be soluble in the oil phase a balance for the surfactant in the continuous phase is governed by Fick's second law [32]:

The flux at the surface is then given by:

$$\left(\frac{\partial C}{\partial z}\right)_0 = \frac{1}{\sqrt{\pi Dt}}(C_{bulk} - C_s) \tag{18}$$

$$\dot{\Gamma}_{transfer} = D\left(\frac{\partial C}{\partial z}\right) \tag{19}$$

scaling the concentration gradient to include the saturation effect:

$$\dot{\Gamma}_{transfer} = \sqrt{\frac{D}{\pi t}}\,(C_{bulk}\,\Gamma^*) \tag{20}$$

and the point value of the mass transfer coefficient is:

$$k_{cts} = \sqrt{\frac{D}{\pi t}} \tag{21}$$

8.2. How to describe the mass transfer at moderate wall shear rates: Reynolds analogy

The idea behind the Reynolds analogy [33] is to relate heat transfer or mass transfer rates to momentum transfer through shear stress. It assumes that elements of fluid are brought from remote regions in the bulk to the surface by the action of turbulent eddies, do not mix with the intermediate fluid along

the way, and instantaneously reach equilibrium upon contact with the interfacial layers [34]. Taylor [35] and Prandlt [36,37] extended the Reynolds analogy to allow for a viscous sub-layer by incorporating the universal velocity profile. The Taylor–Prandlt modification of the Reynolds analogy for heat and mass transfer is used to account for the continuous phase cross-flow increasing the rate of mass transfer via a two stage process [34]. First the surfactant is transferred from the main flow stream to the edge of the viscous sub-layer (δ thick) by momentum, followed by transfer through the sub-layer through molecular motion.

$$\dot{\Gamma}_{transfer} = \frac{\tau_{wall}}{\rho U}\frac{(C_{bulk}\,\Gamma^*)}{1 + \alpha(Sc - 1)}, \quad Sc \equiv \frac{\mu}{D\rho} \tag{22}$$

$$k_{cts} = \frac{\tau_{wall}}{\rho U}\frac{1}{1 + \alpha(Sc - 1)} \tag{23}$$

where U is the average velocity in the continuous phase, τ_{wall} is the wall shear stress, C_{bulk} is the surfactant concentration in the bulk, α is the ratio of the velocity at the edge of the viscous sub-layer to the average velocity (equal to $2.0\,Re^{-1/8}$ for pipe flow), and the Schmidt number, Sc gives the dimensionless relationship Again we can scale the concentration gradient by Γ^* to account for effect the degree of surface saturation has on the driving force for further adsorption.

From continuity this flux is equal to the rate of adsorption of surfactant per unit area. The surfactant flux describes the delivery rate of surfactant, but this does not let us know what the surface coverage actually is because the interface is expanding. This means that the interfacial tension, via the surface coverage is a function of both the mass transfer and expansion history of the droplet.

8.3. Estimation of the diffusion coefficient

Diffusion coefficient is estimated by Stokes–Einstein equation, where k is the Boltzman constant, T is temperature, μ is viscosity of the continuous phase, and a is the length of the molecule [18] which is assumed to be two times R_g.

$$D = \frac{kT}{a\mu} \tag{24}$$

$$R_g \approx M_w^{0.6} \times 10^{-9}$$

The estimated diffusion coefficients and general data for the surfactants presented in this paper are found in Table 1.

9. Quantifying coupled effects of surface expansion and dispersed phase flow

The expansion–transport coupled dynamic interfacial tension can be obtained by using the appropriate model for k_{cts}

Table 1
Estimated diffusion coefficient for polymeric surfactants:

Surfactant	Mwt. (Da)	CMC (mol/m^3)	R_g (m)	D (m^2/s)	Coverage (mol/m^2)
Tween 80[a]	1310	0.1	7.4×10^{-8}	$2.87.1 \times 10^{-11}$	3.0×10^{-6}
Tween 20[a]	1228	0.08	7.1×10^{-8}	5.8×10^{-11}	4.3×10^{-6}
SDS[b]	288.4	6.9	3.0×10^{-8}	1.4×10^{-10}	5.0×10^{-6}

[a] Data from: [45].
[b] Data from: [46].

in the following equation:

$$\frac{d\Gamma}{dt} = k_{cts}C_{bulk}\Gamma^*_{(t)} - \Theta\Gamma_{(t)} \tag{25}$$

This equation can be solved numerically to obtain the surface coverage over time, therefore, a MATLAB program was written to track the geometry of growing droplets, yielding information such as the radius of curvature, average surface age, and surfactant coverage over time, consequently the capillary pressure of the droplet as it grows with time can also be found. With this information a model was developed to include the effect of this coupling on the flow of dispersed phase through the pore. The model of dispersed phase flow was implemented in the MATLAB program and uses a potential flow approach in the form of an electrical circuit analogy, Fig. 5. According to Ohm's law, the voltage drop over a resistor is equal to current through it times its resistance, $V = IR_{ohm}$. Similarly the pressure drop through a flow section is equal to the flow rate, Q times the hydraulic resistance R_{flow} [38]. In this case three resistances to flow were considered:

(1) The pressure in the continuous phase, P_{cts}.
(2) The flow resistance from the membrane:

$$P_{hyd} = QR_{flow} \tag{26}$$

$$\Omega = \frac{8\mu L_{eff}}{\pi R^4_{pore}} \tag{27}$$

where μ is the dispersed phase viscosity, L_{eff} is the effective length of the pore taking the tortuosity into account, and R_{pore} is the pore radius.

(3) The resistance caused by the capillary (Laplace) pressure, P_{cap} across the oil–water interface:
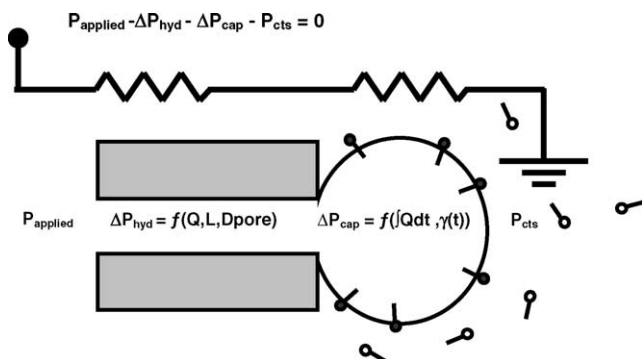

Fig. 5. Circuit analogy showing sources of pressure loss.

$$P_{cap} = \frac{\gamma_{(t)}}{dV}\frac{dS}{dV} \tag{28}$$

where

$$\frac{dS}{dV} = \frac{dS}{dt}\frac{dt}{dV} = \dot{\varepsilon}\frac{1}{Q} \tag{29}$$

In the case of membrane emulsification droplets are forming from pores, which are not necessarily round so instead this general description of the Laplace pressure is used in Eq. (28) [12]. If this definition of Laplace pressure seems unfamiliar recall the following geometric relationships for a sphere:

$$A = 4\pi R^2, \quad \frac{dA}{dR} = 8\pi R, \quad V = \frac{4}{3}\pi R^3, \quad \frac{dV}{dR} = 4\pi R^2,$$

using chain rule $\frac{dA}{dR}\frac{dR}{dV} = \frac{dA}{dV} = \frac{2}{R} \tag{30}$

Yielding the commonly used Laplace equation for a spherical droplet:

$$P_{cap} = \frac{2\gamma_{(t)}}{R_c} \tag{31}$$

where $\gamma_{(t)}$ is the interfacial tension at a particular time and its value is governed by the sum of the effects of diffusion and expansion, and R_c is the radius of curvature of the droplet. For a round pore the dS/dV function can be found analytically, while for non-circular pores this function was found numerically from the surface evolver (described in the next section) which logs the interfacial area data as the volume is incrementally increased.

The area versus volume data is exported from the surface evolver as an ASCII data file, then loaded into MATLAB and used to generate a nth order polynomial fit function $S_n = f(V)$ such that $R^2 > 0.9999$. The derivative of this function with respect to V is subsequently found, dS/dV. Once the loop starts in the MATLAB program, S_n and dS/dV are used to calculate surface area and expansion rates, together with the mass transfer to get the interfacial tension at each time step. The capillary pressure is then calculated from Eq. (28). The program continues and creates an output file of the calculated variables over the droplet formation time.

The interesting aspect to this approach is that it does not assume a constant flow through the pore over the droplet formation time, but rather takes into account how the change in radius of curvature of the droplet and surface relaxation,
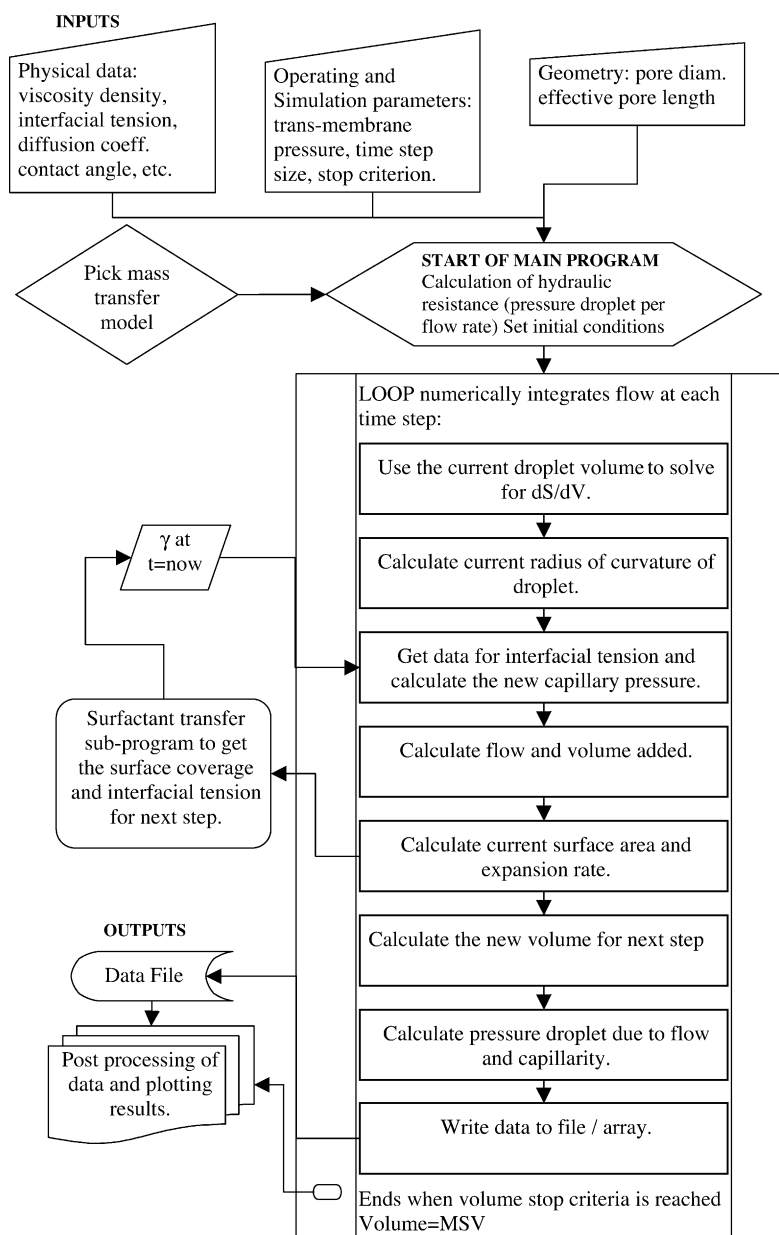
Fig. 6. Algorithm of the MATLAB Program.

decreases the capillary pressure, thus allowing the flow to increase. The algorithm of the program is shown schematically in Fig. 6. The data from the simulation calculations was processed and plots of the pressure losses from flow and capillarity, integrated shear rate, and flow velocity were produced.

This expansion–transport coupled dispersed phase flow model is limited to describing the distribution of pressure losses and to predicting how long it should take to produce droplets of a certain size under given operating conditions. Although this modelling work does reveal some insight into the relative importance of the various parameters it could not predict á priori the final droplet size that would form for a particular set of conditions.

10. Surface evolver: maximum stable volume and final diameter of droplets

The maximum stable volume (MSV) of a droplet attached to a pore of a given geometry was modeled with the help of the Surface evolver, which is an interactive finite element program for the study of surfaces shaped by surface tension and other energies, subject to various constraints [39]. It modifies a given initial interface shape taking into account the requirements of the Gauss–Laplace equation by iteratively moving vertices until a minimum energy configuration is obtained [40]. The initial interface shape, which is decided by the pore geometry, is critical to this modeling method, and thus careful consideration was taken in choosing the system on which
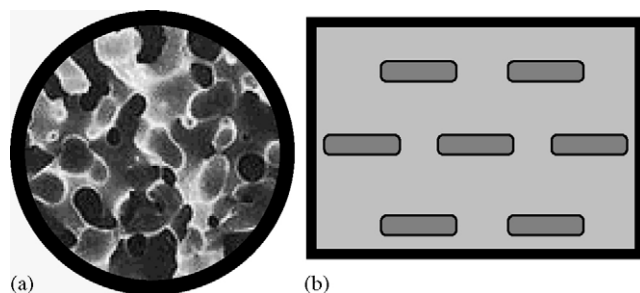
Fig. 7. (a) Illustration of the pore structure of a micro-porous glass membrane (SPG instruction manual, ISE Chemical Company Japan. (b) Schematic sketch of a straight-though micro-channel with rectangular shaped pores.

to test it on. Micro-porous glass and SPG membranes, which have been used to make uniformly sized emulsion droplets, do not have circular pores. They can be described as a network of tortuous ellipsoidal cylinders (Fig. 7a). This non-circular shape increases the droplet's surface area to volume ratio, making the surface be farther away from its lowest energy configuration, which may in fact be the key to their success. Using the micro-porous glass membrane's complex pore shape directly in the surface evolver model is by no means a trivial task. So it was decided that literature data using a pore, which also had a well defined elongated or ellipsoidal shape should be used to reduce the error arising from a poor representation of the membrane's morphology.

Experimental results from Kobayashi and Nakajima [41] were employed to validate the model since they used straight-through micro-channels, which could be seen as an idealised membrane. This data was chosen to test the model for several reasons. The pores used were almost rectangular in shape and this boundary could be represented as a continuous super-elliptical function, making the line integral of wetting energy easier to implement in the surface evolver. Fig. 7b shows a sketch of Kobayashi et al.'s uniform oblong shaped pores were micro-fabricated on a silicon substrate using deep reactive ion etching [42]. In addition to defined geometry, they also give data on the interfacial tension and contact angles for the systems they studied (see Table 2), which were used as input parameters for the surface evolver model.

The model is defined as an initial surface in a data-file, which is executed by the surface evolver program. The Input

parameters of the model, which are adjustable at run-time, are: pore geometry; initial volume of the droplet; oil–aqueous surfactant solution interfacial tension; and contact angle. The surface evolver was used to detect droplet instability by means of eigenvector analysis (for a more detailed explanation see [43]). The droplet volume just before instability is taken to be the maximum stable volume and yields an estimation of the largest droplet, which could form.

The assumptions used in the MSV model are:

(1) The energy arising from interfacial tension on the free surface (oil–surfactant solution interface) is a scalar function of the area.
(2) The energy contribution from the contact angle θ_c between the oil–water interface and the membrane can be represented as a line integral along the pore perimeter with an energy integrand equal to $-\cos(\theta_c \, \pi/180)$.
(3) The energy arising from viscous, inertial and buoyancy effects are negligible.

Calculation of the MSV is carried out increasing the droplet's volume in small increment steps by adding 0.5% of the current volume. After each volume addition, a gradient descent is performed to obtain the surface configuration of lowest energy for that particular volume and given set of constraints; the surface area, volume, and total energy are calculated, as well as the eigenvalues to determine if the droplet is approaching instability. The results from this step are written to the output file and the next volume addition occurs. This process iterates until the droplet becomes unstable. The code automatically takes into account the contributions of the interface to the system's energy, whereas the shape of the boundaries and the wetting energies arising there have to be added by the user by providing appropriate integration coefficients along the contact lines [39]. However, it is well known that a droplet is not popped clean off- there is a certain volume remaining at the pore that includes some of this maximum stable volume.

10.1. Droplet detachment size model: quiescent conditions

Once the maximum stable volume is found, the amount, which breaks away to form the droplet needs to be determined. A here we use a break off model, called the pressure

Table 2
Experimental values from [41] used to verify model

Name	Rc1 (μm)	Rc2 (μm)	γ (mN/m)	θ_c (°)	Diam exp.[*] (μm)	GD-Diam. (μm)
MC1-S1	26.3	7.0	4.4[a]	143	49.0 ± 1.4	55.9
MC1-S2	26.3	7.0	1.9[b]	142	48.9 ± 2.1	49.6
MC1-S3	26.3	7.0	23.4[c]	130	50.3 ± 1.9	61.5
MC1-S4	26.3	7.0	1.4[d]	145	53.2 ± 3.3	54.0
MC2-S1	24.4	4.8	4.4[a]	143	38.9 ± 2.3	36.3
MC2-S2	24.4	4.8	1.9[b]	142	38.1 ± 1.9	35.3

Surfactants: a, 1 wt.% PGFE (pentaglycerol monolaurate); b, 1 wt.% Tween 20 (polyoxyethylene 20 sorbitan monolaurate); c, no surfactant; d, 1 wt.% SE (sucrose monoesterate).

[*] ± coefficient of variation as %.

pinch constraint (PPC) [12], based on the division of the surface into two volumes, a droplet and a segment, which remains attached to the pore mouth. The relative size of these two volumes is such that the resulting radii of curvature of the droplet will maintain an equal Laplace pressure across the surface of both volumes (i.e. $P_{droplet} = P_{attached}$).

The volume of the droplet that breaks off is $V_{droplet}$ and is equal to the maximum stable volume V_{MSV} minus the remaining attached volume, $V_{attached}$. The energy, E_{Total}, and the volumes for all stable surfaces up to the instability point as the droplet grows are logged by the surface evolver. Using this information and the pressure pinch constraint we can solve for the radius of the detached droplet. In the case of a droplet forming from a pore, the pore itself also plays a role in determining the final curvature of the surface. E_{pore} is the energy contribution from the pore itself, and thus is subtracted.

$$V_{droplet} = V_{MSV} - V_{attached} \tag{32}$$

$$R_{droplet} = \sqrt[3]{\left(\frac{3}{4\pi} V_{droplet}\right)} \tag{33}$$

$$P_{droplet} = \frac{2\gamma}{R_{droplet}} = P_{attached} = \frac{\Delta E_{Laplace}}{\Delta V_{attached}},$$
$$E_{Laplace} = E_{Total} - E_{pore} \tag{34}$$

and

$$dE_{Laplace} = -\gamma \, dA \tag{35}$$

Using the pressure pinch constraint we can solve for the radius of the detached droplet (Fig. 8). As the volume of the detaching droplet increases (x-axis in Fig. 8) the Laplace pressure of that droplet decreases, however the larger the detaching droplet the smaller the remaining piece is, and thus the pressure of the corresponding attached surface increases. From the above argument of the PPC we know that these two pressures must be equal and thus we find the volume of the detaching droplet at the intersection of the pressure curves of the two surfaces, P_{drop} and $P_{attached}$.
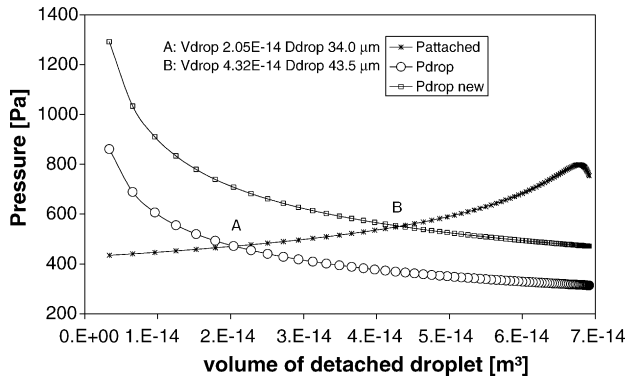

Fig. 8. The pressure pinch constraint droplet size solution for A: quiescent conditions P_{drop}, and B: $P_{drop\,new}$, expansion–transfer conditions. The increase in detached droplet volume between condition A and B is caused by the higher interfacial tension at MSV.

The final droplet size calculated using the pressure pinch constraint applied to the MSV model provides a realistic representation of the system when the effects of transport phenomena are small [12]. As one can see from the assumptions in Section 10, the MSV model does not take into account dynamic effects, thus we will refer to these droplet size predictions as the geometrically determined droplet size. However, as with any process when used in the real world "time is money", thus the output or rate of droplet formation should be maximized, while maintaining the ability to have a predictable and uniform emulsification result. In-order to do this the pressure pinch constraint was developed further to include the effects of expansion-diffusion coupled flow and changes in interfacial tension during droplet formation.

10.2. Droplet detachment size model: dynamic conditions

In order to predict the final detached droplet size we again make use of the pressure pinch constraint, however, now we allow for local changes in interfacial tension caused by mass transfer and surface expansion effects. At this point some statements are made with regard to the surface:

(1) The droplets grow faster at their apex than at the sides near the membrane pore mouth. This assumption is supported by the fact that the mesh (which starts out more or less the same size) is biggest at the apex after evolution (see Fig. 9). Furthermore, the apex has more degrees of freedom than the surface near the constraining contact line.

(2) A higher expansion rate means that the interfacial tension is locally higher where there has been the most expansion. Generally, it is said the mean curvature is equal at all points on a surface at its minimal energy shape. However, in this situation it is proposed that the interfacial tension varies on the surface and that the local curvature
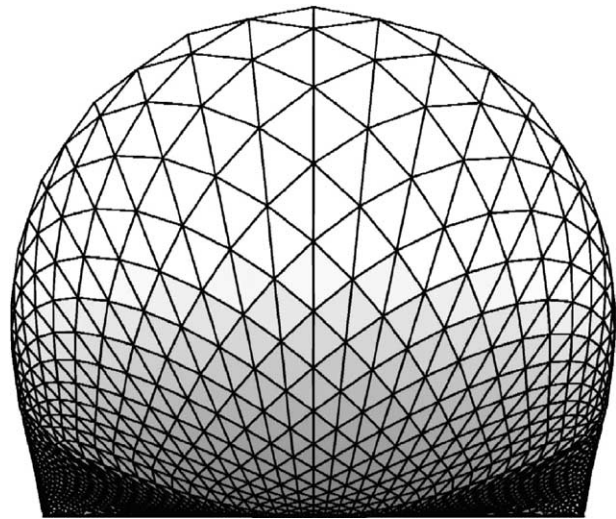

Fig. 9. Image of a surface evolver mesh of a droplet at MSV.

must change in order to satisfy the Laplace equation (Eq. (36)).

(3) From the above two statements it is reasoned that the increase in interfacial tension will be limited to the section of the interface containing the MSV which will detach, and that the pressure of remaining attached segment, P_{attached} segment will be more or less un-changed.

$$P_{\text{Laplace}} = 2H_{xyz}\,\gamma_{xyz} = P_{\text{drop\_new}} \tag{36}$$

$$H_{xyz} = \frac{1}{2}\left(\frac{1}{R_{\max}} + \frac{1}{R_{\min}}\right) \tag{37}$$

where H_{xyz} is the mean curvature and γ_{xyz} is the local interfacial tension at position xyz and $R_{\max}$ and $R_{\min}$ are the local maximum and minimum radii of curvature of the surface.

The increase in Laplace pressure across the interface at MSV was found by the MATLAB program. This new pressure, $P_{\text{drop\_new}}$ is caused by the expansion–transfer coupled changes in interfacial tension described in Section 5. To determine the degree of curvature correction required to satisfy the pressure pinch constraint the increased pressure is compared the corresponding capillary pressure at detachment when there is no mass transfer effect. The new droplet size is calculated based on the required decrease in curvature (increase in radius) of the droplet detaching from the apex to maintain the same pressure in both parts (i.e. so the pressure pinch constraint is upheld Eq. (34)). The result of this is shown in Fig. 8.

$P_{\text{drop\_new}}$ is plotted as a function of detached droplet volume and again as before the intersection of these curves occurs at the volume, which satisfies the pressure pinch constraint and thus droplet will break off at this size.

11. Results and discussion

11.1. Validation of the expansion coupled dispersed phase flow model

The expansion coupled flow model of the dispersed phase was tested using input data from actual membrane emulsification results found in Table 3. The trans-membrane pressures (applied dispersed phase pressure minus continuous phase pressure) geometry, formulation, continuous phase flow conditions, final droplet size were used as input to the MATLAB program. The program tracks the size, flow rate, and surface coverage of the droplets. Since the program integrates over a time step it was necessary to find the size for a step independent result. Here we analysed how the relative maximum dispersed phase flow rate was affected by increasing the number of time steps per second (decreasing the length of the time step). The MATLAB program was run repeatedly using smaller and smaller time steps and the maximum flow rate was recorded. The input parameters were chosen to reflect conditions where the model would be most sensitive to the step size, i.e. when the droplet formation time is small and

Table 3
Data used from [44] to validate expansion-diffusion coupled dispersed phase flow model

Continuous phase	2% Tween 80 in water				
	Wall shear stress: 8 Pa			Cross flow velocity: 1.4 m/s	
Dispersed phase	Rape-seed oil viscosity 58 mPas				
SPG membrane	Diameter:	9.3×10^{-3} m		Length:	0.125 m
	Thickness:	3.5×10^{-4} m		Area:	3.7×10^{-3} m^2
Pore size, dpore (μm)	0.4	1.4	2.5	5.0	6.6
Porosity	0.6	0.6	0.53	0.6	0.58
Tortuosity	1.7	1.7	1.3	2.1	1.7
Process conditions					
Pcritical (Pa)	1.9×10^5	4.8×10^4	2.4×10^4	1.0×10^4	5.0×10^3
Pcritical (Pa)	8.0×10^4	2.3×10^4	1.3×10^4	6.4×10^3	4.9×10^3
Ptm (Pa)	2.0×10^5	5.3×10^5	2.6×10^4	1.1×10^4	5.5×10^3
Flux (l/m^2 h)	0.70	2.3	2.9	4.3	6.6
Active pore ratio (%)	1.9	2.0	1.6	2.0	2.6
d32 (μm)	1.4	4.6	8.5	14.7	23.9
d32/dpore	3.5	3.3	3.4	2.9	3.6
Droplet time (s)	0.6	0.7	0.8	0.9	1.8
Calculated values					
δ^2/Dt [−]	189	162	141	126	63
$\delta^2/Dt \gg \pi$ therefore penetration theory					
MATLAB model's results					
Droplet time (s)	0.66	0.72	0.86	∞	∞
	+10%	+2.8%	+7.5%		
Ptm adjusted (Pa)				1.48×10^4	1.10×10^4
				+34%	+99%

∞ Indicates that no droplet formation occurred at the pressure applied. $P_{\text{critical}} = 2\gamma \cos\theta/R_{\text{pore}}$.
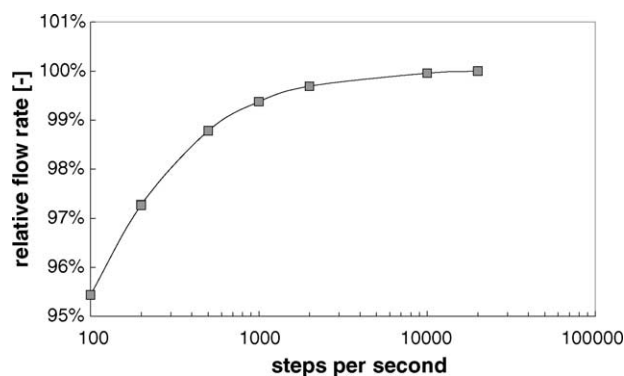
Fig. 10. Determination of the step size to obtain a step-independent solution.

the expansion rate is large. The result of this investigation is shown in Fig. 10. The step size for the step independent result was found to be approximately 5000/s and was used in subsequent calculations.

The model was verified by comparing droplet formation times reported experimentally in the literature [44] to the droplet formation times seen in the simulations using the MATLAB program. The results of this are presented in Table 3. In the first three cases, with the pore sizes 0.4, 1.4, 2.5 μm the predicted droplet formation times deviated from the experimental data by 10, 2.8 and 7.5%, respectively. In the last two cases, the model did not predict any flow through the membrane at the pressure applied. In these two cases the applied pressure was incrementally increased and the simulation repeated until an appropriate droplet formation time was found. This new trans-membrane pressure was noted and compared to the experimental data in Table 2. The model agrees well with the experimental data for the instances tested except that of the 6.6 μm pore. Here the calculated applied pressure was almost twice that was given in the literature. It also should be noted that for this case the δ^2/Dt value was less than half that of the others. Although the criteria for Reynolds analogy is $\delta^2/Dt > \pi$, in reality it can not change abruptly at π to penetration theory, there is of course some transition region between these two models like that seen in equations used for laminar versus turbulent flow. For this particular case $\delta^2/Dt = 63$ and may in fact have been better described by penetration theory or another model. Therefore, the model's deviation under these conditions was not deemed critical.

From analysing the results of the simulations using a range of geometries and applied pressures some general observations could be made: First, under all conditions studied, the Reynolds number describing the dispersed phase flow was less than 10^{-4}, meaning that the flow was laminar and creeping. Secondly, the lower the applied pressure, the higher the effect of the capillary pressure has in regulating the flow. This means that interfacial effects have a greater impact than that predicted by models, which assume a constant dispersed phase flow.

11.2. Validation and results of the geometrically determined droplet size

The model was validated by comparing its predicted droplet diameter to the experimental droplet sizes found in the literature under quiescent conditions given in Table 3. The error of the calculated results ranged from 1.4 to 18% with an average estimation error of 8% [12]. Considering that the experimental data does in itself have a coefficient of variation, CV around 2% this estimation error is quite low.

The geometrically determined drop sized for the two surfactant systems considered in this work are 35.3 μm for Tween 20 and 34.0 μm for SDS. In comparison to the literature data which gives 38.6 μm CV 2.5% and 39.1 μm CV 2.5%, respectively [9]. These predicted droplet sizes differ from the experimental data by 8.5 and 13.5%, an error within the range found previously.

11.3. Checking the soundness of the expanding apex assumption

The surface expansion data generated in the MATLAB program is based on the area versus volume data from the surface evolver. This overall expansion of the surface is based on its total area, however as mentioned above, in Fig. 9 the mesh has obviously not expanded equally, as facets on the top portion of the droplet are larger. It is proposed that this non-isotropic expansion leads to gradients in interfacial tension and thus local changes in curvature which in turn lead to larger droplets at break-off. To see if this assumption is sound we have extracted the area and expansion of each facet at the beginning of droplet growth and at the MSV from the surface evolver. The initial total droplet area (sum of the individual 3600 facets) was approximately 7.3% of the final total area. Once the data for the area, S and expansion, dS were found for each facet they were sorted from smallest to largest dS value. The area and expansion are plotted for each facet in Fig. 11. One can see that there are a large number of small facets (note the logarithmic scale), which do not expand or expand very little, and that most of the area and expansion are attributed to the largest 500 or so facets. To determine how well these large facets represent the calculated overall surface expansion (or in other words how much error is introduced by the assumption) the cumulative normalized mean expansion (CNM-dS) and the cumulative normalized area (CN-S) were calculated and plotted on the right hand axis in Fig. 11. A normalized value of 100% represents the overall expansion rate or total surface area from the MATLAB program, respectively. The plotted values of CNM-dS reach a final value of 152%, meaning that the largest facets have expanded 52% more than the mean expansion rate predicted by the MATLAB program. If we now take a slice of the largest facets such that their CNM-dS value has a mid point at 100%, (i.e. high value at 152%, low value at 48%) we can see that their summed area represents almost 70% of the total drop area. These facets, which are larger than this cut-off (vertical line in Fig. 11) are shown
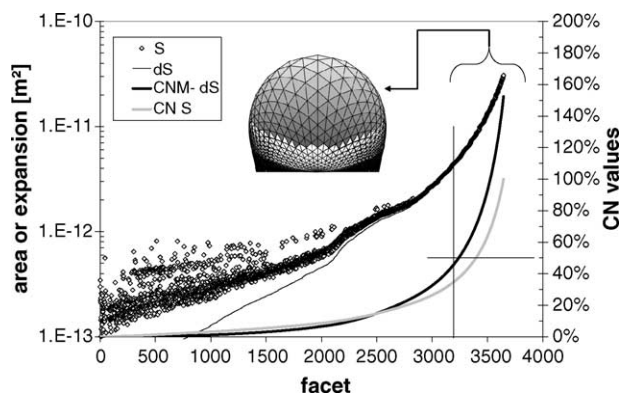
Fig. 11. Plot of area and expansion of individual facets and their cumulative values normalizes by the overall expansion rate found by the MATLAB program. Legend *S*: individual facet area, d*S*: facet expansion, CNM–d*S*: cumulative normalized mean expansion, CN-*S*: cumulative normalised area. Facets are ordered from smallest to largest d*S*. Shaded facets shown in the figure (inset) represent 70% of the total droplet area and together have a CNM-d*S* equal to 100%.

shaded in grey in the Evolver mesh image. Consequently from this analysis it can be concluded that the facets which have expanded the most, together are also most representative of the overall expansion rate, and represent the part of the surface which will break-off into a droplet whose curvature is a direct result of the local rate of expansion.

11.4. Results of modelling the final droplet size including expansion coupled dynamic effects

The amalgamation of the MATLAB program's ability to calculate the mass transfer coupled expansion and surface coverage, with the surface evolver's capability to calculate the maximum stable volume and surface area evolution, allows one to model the final droplet size including dynamic effects of surfactant transport. The MATLAB + evolver program's ability to predict final droplet sizes was tested using literature data found in [9] using the conditions found in Table 4 and penetration theory to describe the continuous phase mass transfer. Figs. 12 and 13 show the results of this simulation for Tween 20 and SDS, respectively. The simulation results agree well with the experimental data, both with respect to shape of the in curve they follow as well as their magnitude. The average error of the simulation prediction compared to the experimental data is 10.4 and 7.4% for Tween 20 and SDS,
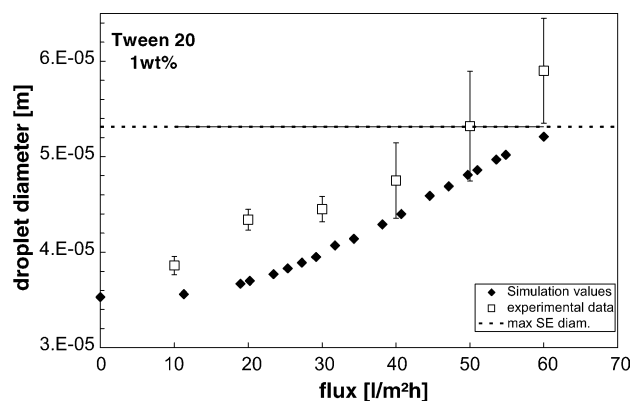

Fig. 12. Droplet diameter as a function of dispersed phase flux for Tween 20 using the conditions in Table 4.

respectively. Bearing in mind that the experimental data's CV ranges from 2.5 to 10.8% for Tween 20 and 3.1 and 14.6% for SDS, the model's predictions can be believed to be quite good. The geometrically determined drop size is also shown in Figs. 12 and 13 as the predicted droplet size (filled diamonds) at zero dispersed phase flux. In reality it is of course impossible to form a droplet without any flux but as per definition of the quiescent condition droplet formation time is infinite thus dispersed phase flux is zero.

The dotted lines labelled Max-SE diam. indicates the largest possible droplet diameter, which could form that does not exceed the MSV for that particular system. In other words droplets forming beyond the Max-SE diam. include effects or mechanisms not included in this analysis. It is also worthy to point out that in the literature data set used [9] there was an additional point for both the Tween 20 and SDS which was not included in Figs. 12 and 13. With the conditions for Tween 20 at 70 l/m^2 h the droplet diameter was approximately 140 μm, CV 42% and for SDS at 100 l/m^2 h the droplet diameter was approximately 165 μm, CV 25%. This data was not included in testing the model because their CV was high and the droplet formation was described as being uncontrolled and jetting under these conditions. What is interesting to point
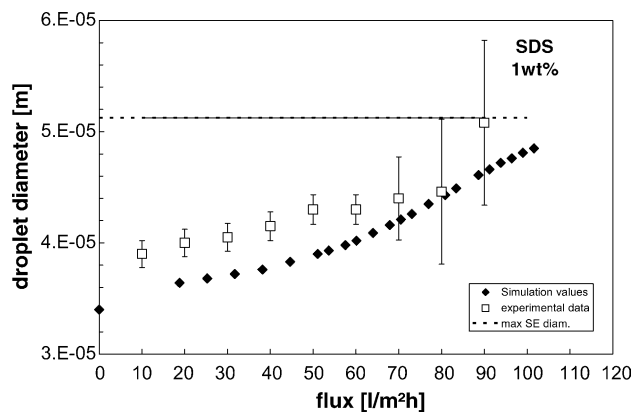

Fig. 13. Droplet diameter as a function of dispersed phase flux for SDS using the conditions in Table 4.

Table 4
Experimental conditions [9] used as input to the MATLAB + evolver model

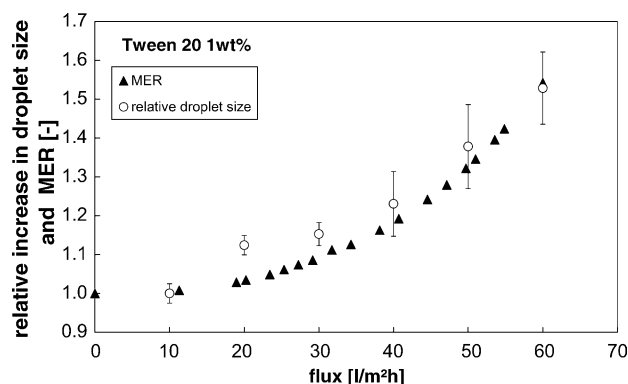| System	SDS (1%, w/w)	Tween 2 (1% w/w)
Pore geometry	Rectangle 48.8 μm by 9.6 μm	Rectangle 48.8 μm by 9.6 μm
Interfacial tension	4.0 mN/m	1.9 mN/m
Contact angle	145°	142°
Cross flow velocity	1.2×10^{-3} m/s	1.2×10^{-3} m/s
Reynolds number	1.1	1.1
Dispersed phase flux	10–100 l/m^3 h	10–70 l/m^3 h

Fig. 14. Increase in relative droplet size and dimensionless mass transfer expansion ratio as a function of dispersed phase flux for Tween 20 using the conditions in Table 4.

out is that the simulations predictions approach the Max-SE diam. at roughly the same flux beyond which the experimental results begin to show uncontrolled droplet formation. The useful aspect to this finding is: if you find that your experimental droplet volumes are larger than the system's MSV for a given geometry and formulation, then the droplets' size and CV can be reduced by either decreasing the flux or increasing the mass transfer rate.

In practical situations it is interesting to look at the increase in droplet size relative to an ideal value as process parameters are changed. Figs. 14 and 15 depict the increase in the experimental droplet size normalized by its low expansion rate value versus dispersed phase flux. It was thought that this increase in droplet size caused by expansion—depletion of surfactant at the interface could be modelled by a dimensionless parameter, the mass transfer expansion ratio:

$$\text{MER} = \sqrt{\frac{\gamma_{\text{detachment}}}{\gamma_{\text{equilibrium}}}} \tag{38}$$

where $\gamma_{\text{detachment}}$ is the final interfacial tension at MSV and $\gamma_{\text{equilibrium}}$ is the interfacial tension found in Table 4. Since the interfacial energy is equal to interfacial tension times the area, the square root was taken to represent it as length-term.
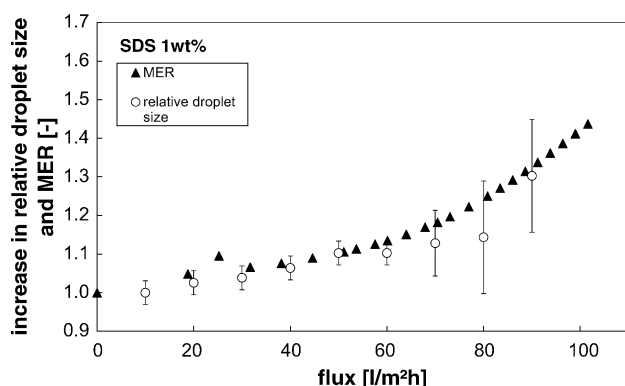

Fig. 15. Increase in relative droplet size and dimensionless mass transfer expansion ratio as a function of dispersed phase flux for SDS using the conditions in Table 4.

The values of MER versus flux are also plotted in Fig. 14 for Tween 20 and in Fig. 15 for SDS. The MER curve of the square root of the relative increase in interfacial tension coincides nicely with the relative increase in droplet size. This discrepancy between the curves is on average 3.1% for Tween 20 and 4.6% for SDS, again values well within the range of the CV of the raw data. The point to this exercise was to show that the increase final droplet size is a direct consequence of interfacial phenomena as it is affected by the dispersed phase flux increasing the expansion-depletion of surfactant.

The differences between the Tween 20 and SDS droplet size increases are consistent with the relative differences in their diffusion and interfacial behaviour. The Tween 20 system allowed for a larger relative increase in droplet size before jetting than did SDS. This can be attributed to Tween 20 higher surface activity which decreased the interfacial tension by 21.1 mN/m compared to SDS's 19 mN/m. The SDS system could withstand higher fluxes, up to 90 $1/m^2$ h versus Tween 20's 60 $1/m^2$ h. SDS is a smaller molecule and thus has larger diffusion coefficient. This means that it can be transported faster to the interface, keeping the interfacial tension lower over a higher range of dispersed phase fluxes and expansion rates.

In Figs. 14 and 15 there appears a small bump in the MER at fluxes 20 and 25 $1/m^2$ h, respectively. This small increase is also seen in the relative droplet size data point for the Tween 20 system. The season for this increase is not completely known. It is however, hypothesized that this flux corresponds to a certain expansion rate where the depletion effects become significant.

12. Conclusions

The transport of surfactants coupled to the expansion rate of the oil–water interface has a significant and predictable effect on the final droplet size in membrane emulsification. The analysis of mass transfer rates, and dispersed phase flux from the perspective of how they effect the interfacial tension has yielded further understanding into this process. The results of the MSV model calculated by the surface evolver predict the final droplet size for a given system and geometry under quiescent conditions. The MSV is also useful to determine the maximum droplet size that can be produced with an acceptable droplet size distribution. The expansion coupled flow model for dispersed phase can predict flux via droplet formation times, as well as determine under what conditions the flow is dominated by the hydrodynamic pressure drop ($P_{\text{TM}} \gg {}_{\text{critical}} = 2\gamma \cos \theta / R_{\text{pore}}$) versus the interfacial tension via the capillary pressure ($P_{\text{TM}} \gtrsim P_{\text{critical}}$). Using interfacing surface evolver's calculated values with the MATLAB program calculating expansion and mass transfer rates allows the prediction of final droplet sizes under dynamic conditions. The extent of the influence of the dispersed phase flux on dynamic interfacial tension was quantified using a dimen-

sionless parameter, the mass transfer expansion ratio, MER. The MER can be used to predict the effect of increasing the depletion of surfactant on the relative final droplet size in membrane emulsification. This new insight into the role mass transfer and surface expansion play in membrane emulsification allow us to now predict à priori the final droplet size that would form for a particular set of conditions, and can lead to better process design methods in the future.

Acknowledgements

Appendix A. Derivation of the surface expansion rate

The relationship between droplet height (h), radius of curvature (R_c) and pore diameter (R_{pore}) is from a right triangle formed with R_c as hypotenuse and R_{pore} as the base shown in Fig. A.1.

$$R_c = \frac{R_{pore}^2 + h^2}{2h} \tag{A.1}$$

The volume of the segment of the sphere, which is the droplet volume exited from the pore.

$$V = \frac{\pi}{6}h(3R_{pore}^2 + h^2) = \int_0^t Q\,dt \tag{A.2}$$

$$Q = \frac{dV}{dt} \tag{A.3}$$

$$\frac{dV}{dh} = \frac{\pi}{2}(R_{pore}^2 + h^2) \tag{A.4}$$

$$\text{Using the chain rule}: \frac{dh}{dt} = \frac{dV}{dt}\frac{dh}{dV} = \frac{2Q}{\pi(R_{pore}^2 + h^2)} \tag{A.5}$$

Since these equations are solved numerically we assume Q is constant over a small time step.
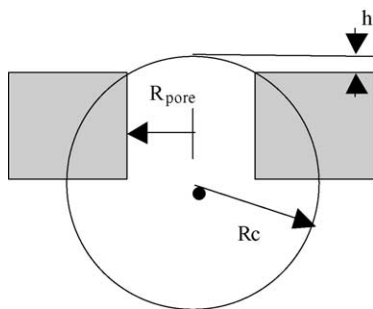

Fig. A.1. Geometrical definition of growing droplet.

To get h as a function of t we can separate the variables and solve for h (real solution only)

$$h = \frac{a^{1/3}}{\pi} - \frac{\pi R_{pore}^2}{a^{1/3}}, \quad \text{where}$$

$$a = \pi^2 3Qt + \pi^2\sqrt{R_{pore}^6\pi^2 + 9Q^2t^2} \tag{A.6}$$

To get the rate of surface area change as a function of time the zone of the spherical segment is considered:

$$S = 2\pi R_c h \tag{A.7}$$

$$S = 2\pi\left(\frac{R_{pore}^2 + h^2}{2h}\right)h \tag{A.8}$$

$$S = \pi(R_{pore}^2 + h^2) \tag{A.9}$$

$$\frac{dS}{dh} = 2\pi h \tag{A.10}$$

The surface expansion rate can be shown in terms of time, flow rate and pore diameter by substituting Eqs. (A.5) and (A.10) into Eq. (A.11).

$$\text{Using the chain rule } \frac{dS}{dt} = \frac{dS}{dh}\frac{dh}{dt} \tag{A.11}$$

$$\dot{\varepsilon} = \frac{dS}{dt} = \frac{4Qh}{(R_{pore}^2 + h^2)} \tag{A.12}$$

References

[1] S.J. Peng, R.A. Williams, Chem. Eng. Res. Des. 76 (1998) 894–901.
[2] H. Schubert, Proceedings of the ICEF 7, 13–18 April 1997, Brighton UK Academic Press, 1997, pp. AA82–AA87.
[3] M. Stang, H. Karbstein, H. Schubert, Chem. Eng. Process. 33 (1994) 307–311.
[4] S.M. Joscelyne, G. Trägårdh, J. Membr. Sci. 169 (2000) 107–117.
[5] C. Charcosset, I. Limayem, H. Fessi, J. Chem. Technol. Biotechnol. 79 (2004) 209–218.
[6] I. Kobayashi, M. Yasuno, S. Iwamoto, A. Shono, K. Satoh, M. Nakajima, Colloids Surf. A 207 (2002) 185.
[7] A.J. Gijsbertsen-Abrahamse, A. van der Padt, R.M. Boom, J. Membr. Sci. 230 (2004) 149.
[8] M. Yasuno, M. Nakajima, S. Iwamoto, T. Maruyama, S. Sugiura, I. Kobayashi, A. Shono, K. Satoh, J. Membr. Sci. 210 (2002) 29.
[9] I. Kobayashi, M. Nakajima, S. Mukataka, Colloids Surf. A 229 (2003) 33.
[10] N.C. Christov, D.N. Ganchev, N.D. Vassileva, N.D. Denkov, K.D. Danov, P.A. Kralchevsky, Colloids Surf. A 209 (2002) 83.
[11] S. Sugiura, M. Nakajima, M. Iwamoto, M. Seki, Langmuir 17 (2001) 5562.
[12] M. Rayner, G. Trägårdh, C. Trägårdh, P. Dejmek, J. Colloid Interface Sci. 279 (2004) 175.
[13] V. Schröder, H. Schubert, Colloids Surf. A 152 (1999) 103.
[14] S.M. Joscelyne, G. Trägårdh, J. Food Eng. 39 (1998) 59.
[15] V. Schröder, O. Behrend, H. Schubert, J. Colloid Interface Sci. 202 (1998) 334.
[16] R. Kumar, N.R. Kuloor, in: T.B. Drew, G.R. Cokelet, J.W. Hoopes, T. Vermeulen (Eds.), Advances in Chemical Engineering, vol. 8, Academic Press, 1970.

[17] G.F. Scheele, B.J. Meister, AIChE J. 14 (1968) 9.

[18] Z. Wang, S. Wang, V. Schröder, H. Schubert, Chin. J. Chem. Eng. 8 (2000) 108.

[19] I. Kobayashi, M. Yasuno, S. Iwamoto, A. Shono, K. Satoh, M. Nakajima, Colloids Surf. A 207 (2002) 185.

[20] C.J.M. Van Rijn, Nano and Micro Engineered Membrane Technology, Elsevier, Amsterdam, 2003, p. 369.

[21] T. Kawakatsu, Y. Kikuchi, M. Nakajima, J. Am. Oil Chem. Soc. 74 (1997) 317.

[22] S. Sugiura, M. Nakajima, M. Seki, Langmuir 18 (2002) 3854.

[23] G.T. Vladisavljevic, U. Lambrich, M. Nakajima, H. Schubert, Colloids Surf. A 232 (2004) 119.

[24] G. De Luca, A. Sindona, L. Giorno, E. Drioli, J. Membr. Sci. 229 (2004) 1999.

[25] J. Eastoe, J.S. Dalton, Adv. Colloid Interface Sci. 85 (2000) 103.

[26] J.R. Campanelli, X. Wang, Can. J. Chem. Eng. 76 (1998) 51–57.

[27] R. Miller, G. Kretzschmar, Adv. Colloid Interface Sci. 37 (1991) 97–121.

[28] P. Joos, Dynamic Surface Phenomena, Utrecht, NL, 1999.

[29] I. Langmuir, Phys. Rev. 8 (1916) 2.

[30] B. von Szyskowski, Phys. Chem. 64 (1908) 385.

[31] R. Higbie, Trans. Am. Inst. Chem. Eng. 31 (1935) 365.

[32] A. Fick, Ann. Phys 94 (1855) 59, Ueber Diffusion.

[33] O. Reynolds, Proc. Manchester. Lit. Phil. Soc. 14 (1874) 947.

[34] J.M. Coulson, J.F. Richardson, Chemical Engineering, vol. 1, sixth ed., Butterworth Heinemann, Oxford, 1999.

[35] Taylor, G.I., N.A.C.A. Rep. Mem. No. 272 (1916) 423.

[36] L. Prandlt, Physik Z. 11 (1910) 1027.

[37] L. Prandlt, Physik Z. 29 (1928) 487.

[38] M. Katti, B. Bal, Physica D 112 (1998) 451.

[39] Brakke, K., "The surface evolver" www.susqu.edu/facstaff/b/brakke/evolver/html/default.htm, (1999).

[40] K. Brakke, Exp. Math. 2 (1992) 141.

[41] I. Kobayashi, M. Nakajima, Eur. J. Lipid Sci. Technol. 104 (2002) 720.

[42] I. Kobayashi, M. Nakajima, K. Chun, Y. Kikuchi, H. Fukita, AIChE J. 48 (2002) 1639.

[43] Brakke, K., Hessian, Eigenvalues, Eigenvectors and Stability in the surface evolver, www.susqu.edu/facstaff/b/brakke/evolver/html/eigentut.htm, 1999.

[44] G.T. Vladisavljevic, H. Schubert, Desalination 144 (2002) 167.

[45] A. McPherson, Crystallization of Biological Macromolecules, CSHL Press, 1999.

[46] T. Nakashima, M. Shimizu, M. Kukizaki, Key Eng. Mater. 61/62 (1991) 513.